DOI: 10.1002/((please add manuscript number))
Article type: Full Paper

Organic Electrochemical Transistors Based on Room Temperature Ionic Liquids: Performance and Stability

Vikash Kaphle[1], Shiyi Liu[1], Chang-Min Keum[1], Björn Lüssem[1]*

[1]Department of Physics
Kent State University
Kent, OH, 44242, USA
[*]*Email:vkaphle@kent.edu*

Organic Electrochemical Transistors (OECTs) are becoming a key device in the field of organic bioelectronics. For many applications of OECTs, in particular for enzymatic sensing, a complex mixture of room temperature ionic liquids (RTILs) combined with other electrolytes is used as a gate electrolyte, making the interpretation of experimental trends challenging. Here, the switching mechanism of OECTs using such RTILs is studied. it is shown that ions smaller in size than the ions contained in the RTIL (e.g. Na^+) have to be added to the ionic liquid to ensure switching of the OECTs. Furthermore, it is shown that OECTs based on RTILs exhibit noticeable gate-bias stress effects and a hysteresis in the electrical transfer characteristics. A model based on incomplete charging/discharging of the effective gate capacitance during operation of the OECT and a dispersion in the ion mobilities is proposed to explain these instabilities, and thus it is shown that the hysteresis can be minimized by optimizing the geometry of the device. Overall, a better understanding of the underlying mechanisms of switching and stability of OECTs based on RTILs is the first step toward various applications such as lactate acid sensors and neurotransmitter recording.

1. Introduction

The inherent flexibility and biocompatibility of organic materials make organic electronic devices well suited for bioelectronic applications. The Organic Electrochemical Transistor (OECT) is one of the most promising organic bioelectronic devices. OECTs are based on conducting polymers such as PEDOT: PSS,[1] which can be processed at low temperatures on

flexible substrates with large areas.[2] Being able to conduct both, electronic and ionic charge, PEDOT:PSS has been widely adopted to transduce ionic signals into electronic signals and to detect ions,[3] metabolites,[4] hormones,[5] DNA,[6] and dopamine,[7] as well as to record brain activity,[8-9] to detect lactate acid,[10] to detect the activity of electrically active cells or tissues,[11] or to drive an active matrix display.[12]

Since the operation mechanism of OECTs is based on doping or de-doping of a conducting polymer, in recent years researchers have been focusing on optimizing the semiconducting materials suitable for OECTs.[13] However, not only does the choice of organic semiconductor influence OECT performance, but the electrolyte has a profound effect as well, the drain current is modulated by the injection of ions from the electrolyte into the organic semiconductor under certain gate bias conditions.[14] For example, in the most common type of OECTs – the depletion mode OECT - the transistor channel is de-doped under application of a positive gate voltage by the injection of cations. Here, the electrolyte determines the ability to inject specific ions present inside the electrolyte into the conducting semiconductor channel. Consequently, the performance of OECTs is linked to how many ions can enter the semiconductor channel and how fast these ions move from the electrolyte to the channel. Hence, the diffusion coefficient of these ions inside the electrolyte as well as the organic semiconductor is expected to have a strong influence on the performance of OECTs. Apart from the electrolyte itself, the mechanical stability of OECTs, its polarization response time, and the solubility of the specific enzymes in the electrolyte are important for many different kinds of applications.[15–17]

Although a wide range of different electrolytes have been proposed such as the ionic liquids 1-ethyl-3-methylimidazolium ethyl sulfate (C2MIM EtSo4)[10] and (1-Ethyl-3-methylimidazolium bis(trifluoromethylsulfony1)imide [EMIM][TFSI], BASF SE),[18] an aqueous sodium chloride (NaCl) solution is the most extensively used.[19-21] However, water-based electrolytes present severe disadvantages: they are susceptible to evaporation, leading to

a change in the ionic concentration, which might limit their long-term use and might cause a degradation of the transport inside the transistor channel. Furthermore, OECTs using water-based electrolytes cannot be easily integrated into wearable sensors, e.g. for monitoring the performance of lactate acid levels in human sweat during exercise.[22]

Room Temperature Ionic Liquids (RTILs) such as C2MIM EtSo4 are an alternative to water-based electrolytes.[23,10] So far, ionic liquids have been used extensively in electrolyte gated organic field-effect transistors.[24–27] In general, the slow polarization response of electrolytes limits the switching speed of these transistors to a few hertz at room temperature. To decrease the polarization time with a large specific capacitance, different ionic liquids were used[28], which show different frequency-dependent double layer capacitances. Furthermore, the field effect mobility of the organic semiconductor increases with decreasing gate capacitance formed by the electric double layers, which was observed by Ono S. et al..[28]

For OECTs employed as enzymatic sensors, Yang et al. used the RTIL as gate electrolyte, which was choosen to be miscible with a water-based phosphate buffer solution (PBS) used in the analyte solution.[23] Later on, Khodagholy et al. used an ionic liquid mixed with PBS in OECT used to sense lactic acid.[10] Zhihui Yi et al. used the ionic liquid (triisobutyl(methyl)phosphonium tosylate) mixed with water in their OECT.[29] Furthermore, ionic liquids can be converted into a solid gel by mixing it with a crosslinker and a photoinitiator, which, for example, was used in lactate acid sensors to prevent the leaching of gel into the human skin.[10]

However, the precise operation of ionic liquids in OECTs and their influence on the working mechanism of OECTs are largely unknown. In particular, as these ionic liquids were mainly used in complex mixtures (containing e.g. PBS), determining which ionic species was mainly responsible for de-doping the semiconducting films is challenging. Furthermore, the presence of a multitude of different ion species makes interpreting their individual influence on the OECT behavior challenging.

Here, we study the influence of an ionic liquid, C2MIM EtSo4, on OECT operation. We observe experimentally that the RTIL itself is not sufficient to de-dope the channel in the OECT, i.e. OECTs based on an ionic liquid alone do not modulate the drain current properly. However, the RTIL provides a stable mixture when mixed with water-based electrolytes. Overall, the mixture of the ionic liquid C2MIM EtSo4 and either NaCl or PBS constitute a new class of electrolytes that provide transistors with high on/off ratios minimumal gate leakage, and a stable interface when integrated into wearable or flexible systems.

However, we observe that the use of ionic liquids introduces instabilities in the OECTs, including, a hysteresis in the transfer characteristic and gate bias stress effects. Considering that OECTs hold great promise as technology for in-vivo measurements or implantable sensors[8,30], an extremely high device stability and reliability is essential. Understanding potential sources of instabilities and devising strategies to minimize the instabilities is the first step toward a realistic application of OECTs in these areas.

Here, we propose that the observed instability is due to migration of slowly moving ions into the active channel, which is most likely the cations of the RTIL. This migration does not lead to a permanent damage of the device, i.e. the shift in the transfer characteristics is reversible. Furthermore, the hysteresis can be minimized by either optimizing the geometry of the device or by cross-linking the electrolyte, turning it into a gel.

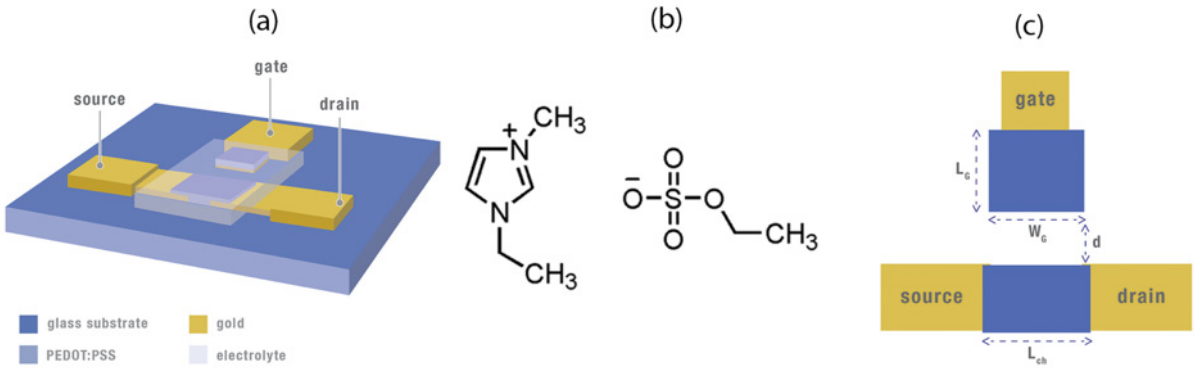

Fig 1: (a) Sketch of the design of the OECT used in this study, (b) Chemical structure of C2MIM EtSo4 used as gate electrolyte, (c) Top-view of the OECT indicating the gate, gate/channel distance d, and the gate area $A = L_G W_G$.

2. Result and Discussions

Figure 1 shows the design of the OECT used here (a) and the chemical structure of the ionic liquid C2MIM EtSo4 (b) employed as the gate electrolyte. The planar arrangement of source, gate, and drain electrodes allow us to precisely tune the distance and length of the ionic conductor (cf. Figure 1c)), which is later on used to determine the origin of the hysteresis observed in the transfer characteristic of the devices. Otherwise, the transistor follows the design of OECTs as proposed by Khodagholy et al..[10] Thermally deposited gold electrodes are formed by photolithography. PEDOT:PSS is spin-coated on top of the electrodes and is structured by OSCoR 4000 (Orthogonal Inc.) to cover the gate area and to define the transistor channel. All devices are characterized inside a nitrogen filled glovebox. More details of device processing are given in the experimental section.

The transfer characteristics of a device using only the ionic liquid C2MIM EtSo4 as gate electrolyte is shown in Figure 2 (black line). It can be seen that this choice of electrolyte leads to a very poor operation of the device with almost no gate modulation.

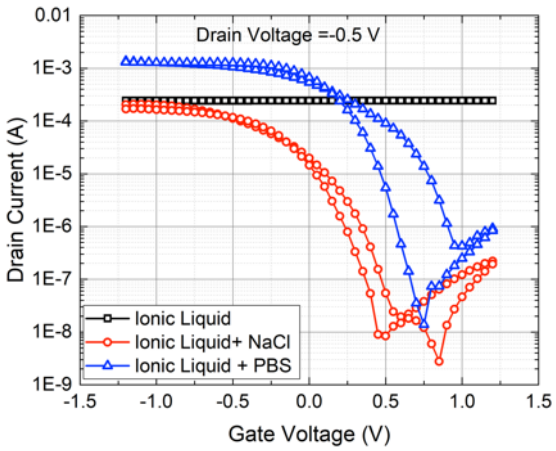

Fig 2: Comparison of transfer characteristics of OECTs based on only RTIL C2MIM EtSo4 only, on the RTIL *mixed with 100 mM NaCl at a 4:1 ratio, and RTIL (the monomer NIPAAm, the crosslinker MBAAm and the*

photoiniator dimethoxy-phenylacetophenone DMPA were added here to allow for crosslinking the electrolyte later on), mixed with 100 mM PBS at a 4:1 ratio. The transfer characteristics are measured at $V_{DS} = -0.5\,V$.

However, if either an aqueous solution of NaCl (100 mM) or PBS (100 mM) is added to the ionic liquid, significanly higher ON/OFF ratios of up to three orders of magnitude are reached (cf. Figure 2). The maximum transconductance of the device using the ionic liquid:PBS mixture exceeds 2 mS, which is comparable to the highest reported transconductance of lateral OECTs using a pure NaCl solution as the electrolyte.[31] Although the absolute transconductance depends on the particular device geometry, this results indicates that OECTs using ionic liquids mixed with PBS as the electrolyte show a sufficient performance for later applications.

Figure 2 indicates that the cation of the RTIL C2MIM EtSo4 is not effective enough to de-dope the layer on its own. This emplies that smaller ions contained in PBS such as Na^+ or Na^+ / K^+ have to be added to the electrolyte to enable switching in OECTs. The radius of ions (including the solvation shell) inside a medium is related to their mobility as[32]

$$\mu = \frac{|z|e}{6\eta r} \qquad (1)$$

In which z represents the charge of the ions, e is the elementary charge, and η the viscosity of the solution.

Therefore, it can be assumed that $C2MIM^+$ ions move significantly slower inside the organic semiconductors compared to for example, Na^+ solutions, leading to a weaker de-doping effect and hence a lower switching ratio. However, Equation 1 shows that the ionic conductivity depends not only on the size of the ions but also the viscosity of the electrolyte, which therefore can contribute to the poor gating effect of the transistors without the added NaCl or PBS as well. Other effects, such as a structural change inside the transistor channel caused by the swelling of the electrolyte due to the addition of a water based PBS might contribute to the observations discussed here. However, as we will show later prolonged heating and drying of the device does

not change its electrical performance significantly, indicating that structural effects due to water uptake into the channel are minimal.

2.1. Origin of Hysteresis in Transfer Characteristics

Figure 2 shows a significant hysteresis between the forward and backward scan, if a mixture of an ionic liquid with an aqueous solution of NaCl or PBS is used. Hysteresis effects are widely observed in conventional organic field-effect transistors and are often explained by charge trapping at the oxide channel interface.[33–35] However, this explanation cannot be applied to OECTs because of the permeable nature of their channel and their overall different working mechanism.

The OECTs plotted in Figure 2 are operated on a potential range from $V_{GS} = -1.2\ V$ to $1.2\ V$ with $V_{DS} = -0.5\ V$, which is larger than in most reports on OECTs. This voltage range, which is applied to reach the full ON/OFF ratio of the transistors, exceeds the voltage that can induce hydrolysis of water at the drain. Considering that water-based electrolytes (NaCl and PBS) were mixed into the RTIL, the observed hysteresis might be caused by initiating hydrolysis. Indeed, the hysteresis increases with increasing scan ranges, as is shown in Figure 3a, which plots the transfer characteristics of an OECT using the ionic liquid mixed with a 100 mM NaCl solution in water in 4:1 ratio.

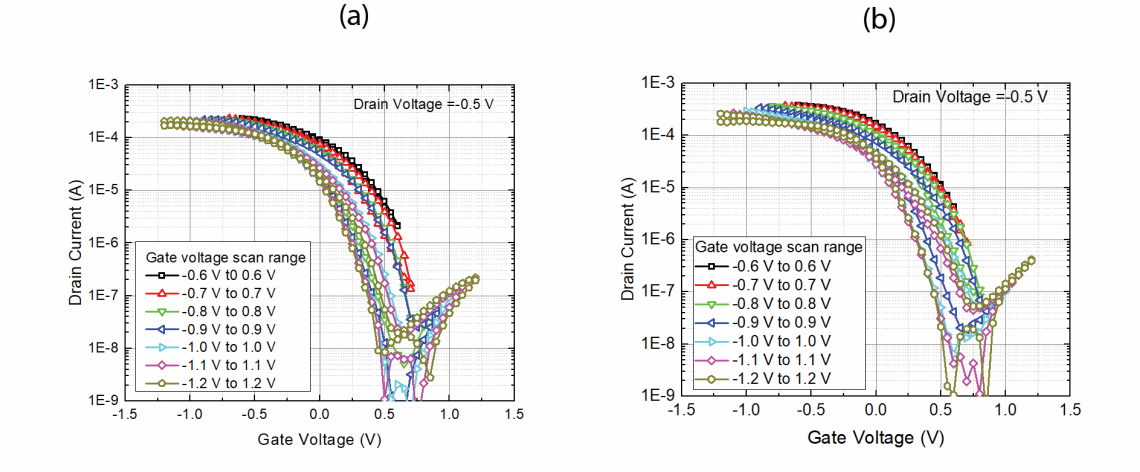

Fig 3: (a) Transfer characteristics of OECTs using the ionic liquid C2MIM EtSo4 mixed with a 100mM aqueous NaCl solution at a ratio of 4:1. The transfer characteristics are measured subsequently with increasing scan range, but without annealing the device. Increasing the scan range leads to an increase in hysteresis. (b) Transfer characteristics of the same OECT shown in (a), but after annealing the device at 120 °C for two hours to minimize the water content. No significant changes from the original devices are observed.

In oder to test if hydrolysis occuring in the electrolyte has a significant impact on the transfer characteristics, the device was annealed at 120°C for two hours and measured in a dry, nitrogen filled glovebox to minimize the water content in the electrolyte. As shown in Figure 3b, the transfer characteristics do not change significantly and the hysteresis does not decrease, which indicates that despite the voltage range dependency, the effects of hydrolysis of the water contained in the electrolyte are not significant.

To further study the origin of the hysteresis, the gate area $L_G \times W_G$ defined by the overlap of PEDOT:PSS and the gold electrodes as shown in Figure 1c is varied. The result of this variation is presented in Figure 4a. Previously, Cicoira et al. reported that the size of the gate electrode changes the characteristics of the transistors, i.e. larger gate areas lead to a smaller voltage drop across the gate/electrolyte interface and hence an increased gate modulation.[36] In Figure 4a, it is observed that the hysteresis becomes smaller for larger gate areas, e.g. the hysteresis decreases by approx. 0.4 V for a 60% increase in gate area in the saturation region.

Additionally, the transfer characteristics of devices with different distances between the gate and the PEDOT:PSS channel d are shown in Figure 4b. It can be seen that the hysteresis is smaller for gates which are closer to the channel even if the area of the gate is smaller. These results again show that hydrolysis has only a minor or no influence on these measurements as hydrolysis should depend solely depend on the applied potential difference regardless of the length of the electrolyte.

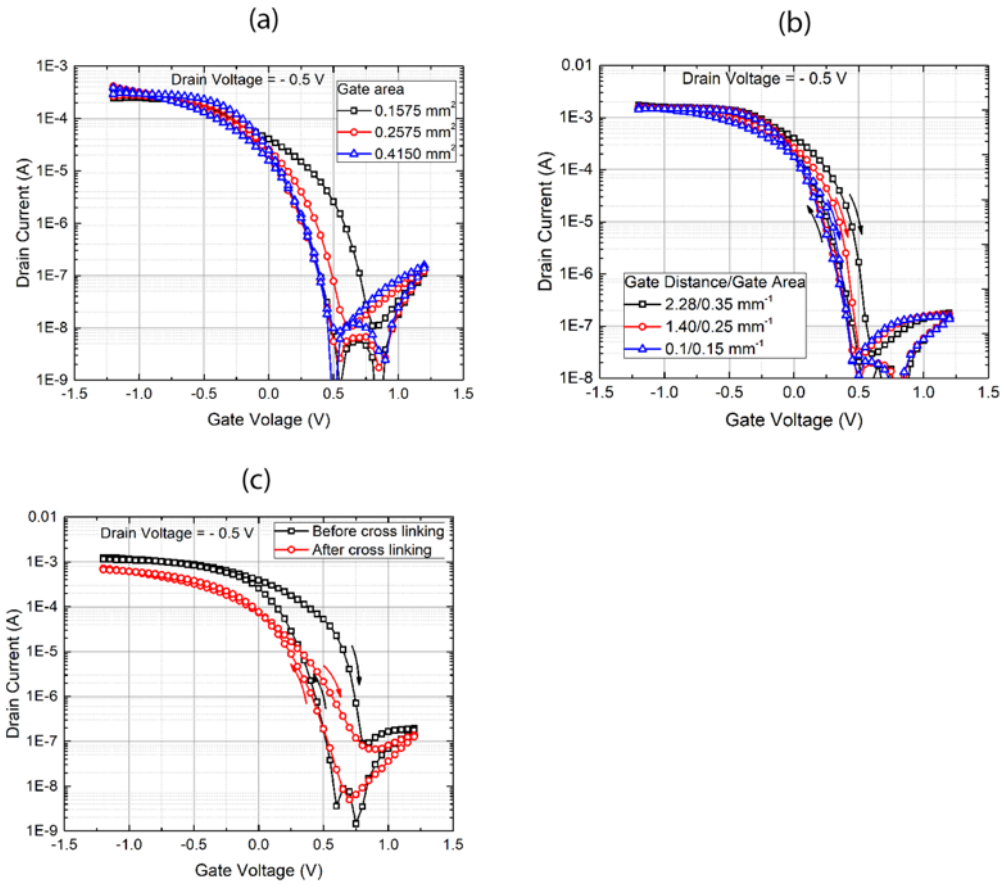

Fig 4: (a) Transfer characteristics of OECTs with varying gate area as defined in Figure 1c keeping the gate distance d *at 100 µm and the channel length L at 200 µm, (b) Transfer characteristics of OECTs with varying ratios of gate distance to gate area d/A.* d *varies from 100 µm, to 1440 and then to 2880 µm. A varies from 0.1575 mm², to 0.2575 mm² and then to 0.3575 mm². All transistors have a channel length L of 100 µm, (c) Transfer characteristics of the OECT before and after cross-linking by 2 min exposure to UV with a 100 µm channel length. The ionic liquid mixed with 100 mM PBS in 4:1 ratio along with crosslinker and monomer is used for all measurements.*

Overall, Figure 4a and 4b indicate that the hysteresis scales with the resistance of the electrolyte, i.e. it decreases when the distance between the gate electrode and channel decreases, and the

the gate area increases. Bernards et al. proposed a model describing OECT behavior and the de-doping process in which the electrolyte is represented as a resistor (R_{ion}) connected with a capacitor (C_G) in series.[14] However, since a mixture of electrolytes is used in our OECTs, the original model of Bernards et al. has to be adapted for the mixture. To account for the different ionic species and separate ionic systems. RC elements representing the ionic resistance and ability to inject cations into the organic semiconductor of the different cations have to be included. These resistances can have strongly varied magnitudes, as already shown by the weak switching of devices using a pure RTIL in Figure 2.

These considerations lead to the equivalent circuit model of the OECT sketched in Figure 5. In Figure 5, $R_{ion,1}$ and $R_{ion,2}$ represent the migration of e.g. Na^+ and $C2MIM^+$ cations inside the electrolyte and organic semiconductor for the sake of simplicity, but more resistances for other ions can be added. C_{Gn} describes the number of injected cations of a particular species inside the organic semiconductors per unit voltage, and the OECT is described by a voltage-controlled current source $I_D = g_m V_{GS}$.

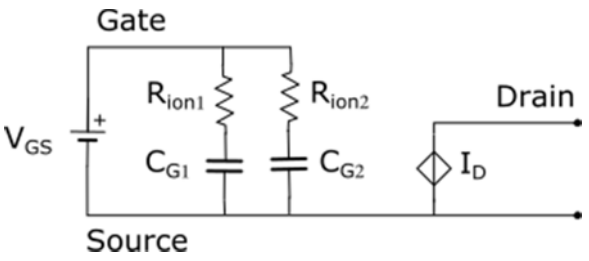

Fig 5: Equivalent circuit of OECTs used to describe the origin of hysteresis.

Using the equivalent circuit model, the response of the device to a voltage ramp $V_{GS}(t) = R_0 \varepsilon(t) t$ ($R_0 = {}^{dV}/_{dt}$: voltage scan rate, $\varepsilon(t) = \begin{cases} 1, t \geq 0 \\ 0, t < 0 \end{cases}$) as applied during measurement of the transfer characteristics, can be calculated. The voltage drop across a capacitor C_{Gn} becomes

$$V_{Cn}(t) = \varepsilon(t) R_0 \left[t - \tau_n \left(1 - exp\left(-\frac{t}{\tau_n} \right) \right) \right] \quad (2)$$

$$\tau_n = R_{ion,n} C_{Gn} \quad (3)$$

Treating the OECT as a voltage controlled current source with a transconductance g_m, the drain current I_D is related to V_{Cn} as

$$I_D = \sum_n g_{m,n} V_{cn} \quad (4)$$

Equation 2 shows that the response of the transistor to the voltage ramp depends on the time constant $\tau_n = R_{ion,n} C_{Gn}$ of the different cations. In the case of Figure 5, the mixture of the RTIL C2MIM EtSo4 and NaCl is described by the time constants of the Na^+ and of the $C2MIM^+$ cations. If these time constants are smaller than the timescale of the measurement (i.e. $\tau \ll T; T = R_0 V_{max}$), the response simplifies to $V_{Cn}(t) \approx R_0 \varepsilon(t) t = V_{GS}(t)$, i.e. the voltage drop across the capacitor is propertional to the external applied voltage. However, if the time constant of a slower ionic species (e.g. $C2MIM^+$) is in the range of T, the exponential factors in Equation 2 cannot be neglected, i.e. charging the RC element is slower than the experimental timescale. Hence, if the voltage is ramped down during the measurement cycle, the drain current measured in the forward scan does not equal the current in the reverse scan, i.e. a hysteresis is observed. This model is able to explain the dependence of the hysteresis on the length and area of the ionic semiconductor, as a smaller distance or larger area leads to a smaller R_{ion} and hence a smaller time constant.

To show that not only the geometric dimensions of the electrolyte have an influence, but the transport properties of the ionic conductor affect it as well, we cross-link the electrolyte, which transforms the electrolyte into a gel and improves the mechanical stability of the device.[10] Furthermore, cross-linking is expected to provide a better ionic transport toward the semiconductor channel.[37-38] Indeed, as shown in Figure 4c crosslinking the RTIL leads to a significant reduction in hysteresis. Apart from the decrease in hysteresis, the on current degrades slightly, which can be explained by the degradation of the semiconductor under exposure to UV while cross-linking the electrolyte.

2.2 Gate Bias Stress Effect in Organic Electrochemical Transistor

For organic field-effect transistors, a hysteresis in the transfer characteristic is often accompanied with gate stress bias effects, i.e. with a shift in the threshold voltage after the application of a constant bias to the gate. In fact, the model proposed in Figure 5 implies that gate bias stress effects should be visible as well in OECTs, in particular due to larger ions moving slowly inside the organic semiconductors.

Although gate bias stress effects have been intensively studied for organic thin film transistors[39] and organic electrolyte gated transistors,[40–42] they have not been thoroughly been investigated for organic electrochemical transistors yet.

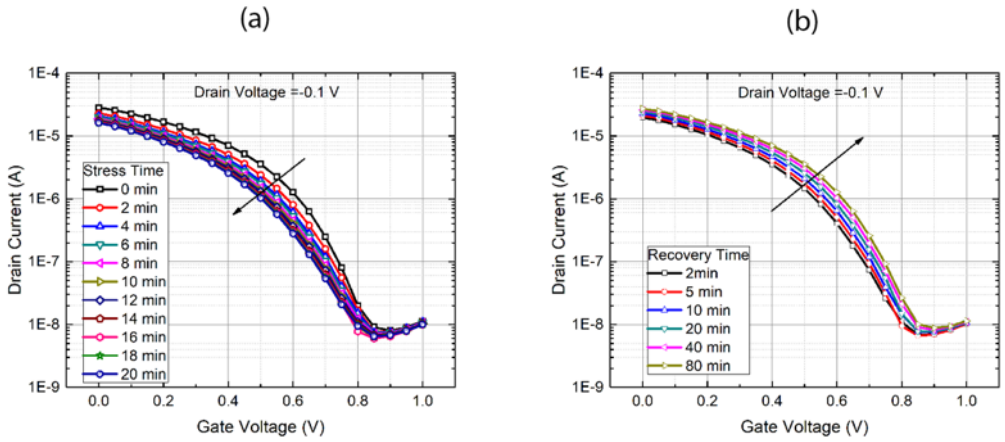

Fig 6: (a) Shift of the transfer characteristics with time if OECTs are stressed at $V_{GS} = 0.1\,V$ *and* $V_{DS} = -0.1\,V$ *(b) Recovery of the transfer characteristics after removal of the stress.*

The results of a gate bias stress measurement are shown in Figure 6 and Figure 7. The OECTs are stressed at three different conditions: at a gate voltage of 0.1 V and a drain voltage of -0.1 V(in the linear region), at a gate voltage of 0.5 V and a drain voltage of -0.1 V, and at a gate voltage of 0.8 V and a drain voltage of -0.1 V (in the saturation region) for 20 minutes.

All measurements show a shift in the transfer characteristics toward higher voltages, i.e. the pinch-off voltage is increased (the shift for stressing in the linear regime is shown in Figure 6a). To quantify the shift in the pinch-off voltage, we follow the model of Bernard.[14] The drain current is given by:

$$I_D = G\left(1 - \frac{V_G - V_{D/2}}{V_P}\right)V_D \quad (5)$$

$$I_D = -G\frac{(V_G - V_P)^2}{V_P} \quad (6)$$

For the linear and saturation regions, respectively. Here, G is the conductance of the channel at zero gate voltage and V_P is the pinch-off voltage of the device.

Following Equation 6, the pinch-off voltage is calculated as the intersection of a linear fit of the square root of the drain current in the saturation region with the gate voltage axis. The results for all stress conditions are shown in Figure 7a. Overall, the shift is stronger for higher gate voltages than for smaller ones.

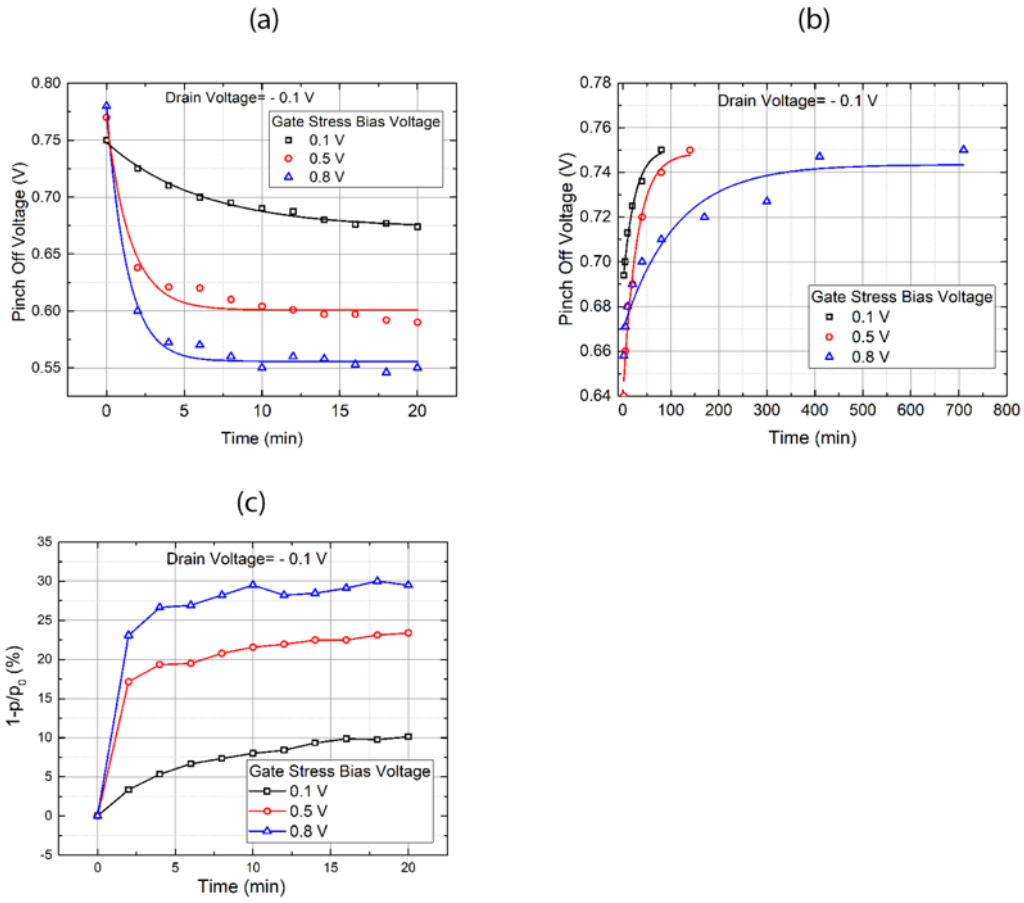

Fig 7: (a) Shift of pinch off voltage with time. The solid line is an exponential fit which follows $V_p(t) = A + B \times exp(-C \times t)$ *(A=0.55 V; B=0.22 V; and C=0.76 min*$^{-1}$ *for* $V_{GS} = 0.1V$ *and* $V_{DS} = -0.1V$*; A=0.60 V; B=0.17 V; and C=0.65 min*$^{-1}$ *for* $V_{GS} = 0.5V$ *and* $V_{DS} = -0.1V$*; A=0.67 V; B=0.075 V; and C=0.16 min*$^{-1}$ *for* $V_{GS} = 0.8V$ *and* $V_{DS} = -0.1V$*). (b) Recovery of the pinch off voltage with time fitted by the function* $V_p(t) = A + B \times exp(-C \times t)$ *(A=0.75 V; B=-0.06 V; and C=0.04 min*$^{-1}$ *for* $V_{GS} = 0.1V$ *and* $V_{DS} = -0.1V$*; A=0.74 V; B=-0.11 V; and C=0.035 min*$^{-1}$ *for* $V_{GS} = 0.5V$ *and* $V_{DS} = -0.1V$*; A=0.74 V; B=-0.07 V; and C=0.009 min*$^{-1}$ *for for* $V_{GS} = 0.8V$ *and* $V_{DS} = -0.1V$*). (c) Percentage change in concentration of free holes inside the PEDOT:PSS channel for the different gate stress conditions.*

The plot of the pinch-off voltage in Figure 7a shows an exponential decrease with stress time. Fitting the pinch-off voltage for all stressing conditions with a mono-exponential function leads to time constants of 78 s for gate voltage 0.1 V and drain voltage -0.1 V (linear regime), 91 sec for gate voltage 0.5 V and drain voltage -0.1 V, and 375 s for gate voltage 0.8V drain voltage -0.1V (saturation regime).

Again, using the standard model of Bernard et al.[14] the pinch off voltage is given by

$$V_P = \frac{qp_0}{C_G} \tag{7}$$

Where p_0 is the density of free charges in the PEDOT:PSS layer present in the channel, which equals the density of ionized or active dopants N_A^- if no cations are present inside the organic semiconductor, q is the elementary charge and C_G the gate capacitance. Assuming that the gate capacitance is constant, Equation 7 indicates that the pinch off voltage is directly proportional to p_0.

If one assumes a dispersion in the mobility of cations inside the PEDOT:PSS layer following the discussion of the hysteresis in the preceding section, some slowly moving ions (for example the cation of the electrolyte C2MIM$^+$) will remain inside the PEDOT:PSS layer even after the removal of the gate voltage. Hence p_0 is reduced to

$$p_0 = N_A^- - N_C(t) \tag{8}$$

with $N_C(t)$ equal to the density of remaining cations inside the PEDOT:PSS layer. Equation 7 together with Equation 8 leads to a shift in the pinch-off voltage. Figure 7c plots the relative

change in effective density of free charges p_0 obtained using Equation 8. As expected, the density of free charges p_0 decreases with increasing gate potential, which corresponds to an increased density of remaining cations $N_C(t)$ inside the PEDOT:PSS channel. We calculate the fraction of hole concentrations are approximately 10%, 22% and 30% due to gate stress bias of 0.1 V, 0.5 V and 0.8 V respectively, as shown in Figure 7c.

Most interestingly, the transfer characteristics recover when the gate bias stress is removed, which is shown in Figure 7b. The detailed description of the relaxation measurements is given in the measurement protocol.

Figure 7b indicates that the recovery of the devices follow a mono-exponential dependency and also with a time constant of 25 min for gate voltage 0.1 V drain voltage -0.1 V (linear regime), 28 min for gate voltage 0.5 V drain voltage -0.1 V and 111 min for gate voltage 0.8V drain voltage -0.1 V (saturation regime). It shows that the recovery time is higher for devices stressed in the saturation region compared to the devices stressed in the linear region, which might be explained by ion migration deeper inside the active channel due to higher gate stress bias.

3. Conclusion

The working mechanism of OECTs with PEDOT:PSS channels based on the RTIL C2MIM EtSo4 as an electrolyte is studied. It is shown that the RTIL has to be mixed with a solution of smaller ions in order to obtain a strong switching effect, indicating that the larger cation of the RTIL $C2MIM^+$ is too large to effectively de-dope the organic semiconductor PEDOT:PSS.

Two instabilities in the transfer characteristics of OECTs based on PEDOT:PSS are found : a hysteresis in the drain current between the forward and backward sweep and a shift in the transfer characteristics due to gate bias stress. A systematic variation in the device dimensions indicates that the hysteresis is related to the ionic resistance of the different ions. Using a simple equivalent circuit model of the OECT shows that the hysteresis can indeed be explained by the

large time constant $\tau = R_{ion}C_G$ of the migration process of either the C2MIM$^+$ of the RTIL or even of the Na^+ ion into the organic semiconductor.

The observed shift in the transfer characteristics due to gate bias stress, i.e. the shift in pinch-off voltage, has been rationalized by de-doping of the organic semiconductor by these slow-moving ions, which remain inside the organic semiconductor even after removal of the gate bias stress. However, as expected, this effect is reversible, which emphazises that the gate bias stress does not permanently degrade the semiconductor materials.

The results discussed here present a first insight into the mechanisms limiting the stability of OECTs based on PEDOT:PSS. However, even with small improvements in the ion conductor (i.e. by cross-linking the ion-gel), the OECT can be turned into a highly stable device. Furthermore, the observed shelf-life time (only 10% degradation in drain current over 30 days of storage at room temperature, Figure S1), and the high temperature stability of up to 150 ºC, Figure S2, will allow for many applications of these transistors.

Apart from understanding the origins of hysteresis and gate bias stress effects in OECTs, the results shown here are closely related to artificial synapses based on electrochemical systems as described by Xu et al.[43] or van de Burgt et al.[44]. These recent advances show that controlling ion migration in a mixed electron/ionic conductor can be used to model essential pre-requisites for neuromorphic computing such as short- or long-term potentiation.

4. Experimental Section

Device fabrication: The electrodes are structured by photolithography. To obtain the electrode‘s structure, the photoresist AZ 2020 is spin-coated at 3000 rpm on the cleaned glass substrate and subsequently baked at 110°C on a hot plate. The photoresist is exposed to UV by using Karl SUSS Mask Aligner, post-baked at 110 °C and developed for 2 minutes in MIF 300

developer in sequence. The metal electrodes are deposited by vacuum deposition of 10 nm chromium followed by 50 nm of gold onto photoresist-patterned glass substrates. The source, drain and gate electrodes are structured by lift-off of the photoresist in acetone. The channel length varies from 100 µm to 400 µm, while the channel width is kept constant at 150 µm.

PEDOT:PSS based gate electrodes are structured by lithography, which are alternatively arranged along with channels. 20 ml of PEDOT: PSS (PH1000 provided by Clevios) is mixed with 1 ml ethylene glycol and 50 µl dodecyl benzene sulfonic acid to enhance the conductivity of the semiconductor. PEDOT:PSS thin films are deposited onto the substrates by spin coating at 1000 rpm. PEDOT:PSS is subsequently baked at 130 ° C in a nitrogen filled glove box (oxygen and humidity levels below 0.1ppm) and rinsed with DI water to remove any excess low molecular compounds.

The PEDOT:PSS channel and gate is structured by the photolithographic process using photoresists, developers and strippers based on fluorinated materials. These materials are ‘‘orthogonal’’ to both polar and nonpolar solvents and do not damage the organic materials during the patterning process[45-47]. OSCoR 4000, the orthogonal photoresist of Orthogonal Inc. is spin-coated on top of PEDOT:PSS at 1000 rpm. The substrate is annealed at 90° C for 1 min and exposed to UV using Karl Suss Mask Aligner MJB4. The substrate is subsequently annealed at 90° C for 1 min and developed for 2 minutes by using Orthogonal developer. Oxygen plasma etching at 200 W for 1 minutes in Oxford 80 Plasma Lab is used to remove PEDOT:PSS except for the channel and gate region. Finally, stripper (Orthogonal Inc.) is used to remove the remaining orthogonal resist on top of the channel and gate electrodes.

Preparation of electrolyte: The preparation of the ion gel follows the procedure published by Khodagholy et al.[10] C2MIM EtSO4 purchased from Sigma Aldrich. The ion gel is mixed with 100 mM NaCl or 100 mM PBS in 4:1 ratio to obtain the RTIL. To be able to cross-link the ion gel we add a monomer (N-isopropylacrylamide, 10 mg), cross linker (MBAAm, 5 mg), and

photoinitiator (DMPA, 10mg) to 2 mL of the RTIL. Finally, we place the electrolyte on top of the channel and gate area of the device. In some devices, we expose the gel to UV light for 2 minutes to cross-link. All electrical characterization is carried out by a Keithley 4200 semiconductor analyzer inside a nitrogen filled glovebox.

Measurement protocol: The transfer characteristics are measured by sweeping the gate voltage from -1.2 V to 1.2 V at a fixed drain bias -0.5 V unless specified. The sweeping direction is from negative gate voltage to positive gate voltage and then back to the negative voltage. For the stress bias test, the measurements of the transfer characteristics start at zero gate voltage and the voltage is swept up to 1V to avoid additional stress at negative bias. To measure the recovery of the devices after gate bias stress, the transistors are stored in the protective environment without applying any bias voltage, until the transfer characteristics are measured at the specified time interval.

Acknowledgements

Device were prepared at the Prototype Facility of the Liquid Crystal Institute, Kent State University.The authors gratefully acknowledge funding from the National Science Foundation (Grant # 1750011).

References

[1] D. Khodagholy, M. Gurfinkel, E. Stavrinidou, P. Leleux, T. Hervé, S. Sanaur, G. G. Malliaras, *Appl. Phys. Lett.* **2011**, *99*, 163304.

[2] W. Lee, D. Kim, J. Rivnay, N. Matsuhisa, T. Lonjaret, T. Yokota, H. Yawo, M. Sekino, G. G. Malliaras, T. Someya, *Adv. Mater.* **2016**, *28*, 9722.

[3] P. Lin, F. Yan, H. L. W. Chan, *ACS Appl. Mater. Interfaces* **2010**, *2*, 1637.

[4] C. Liao, C. Mak, M. Zhang, H. L. W. Chan, F. Yan, *Adv. Mater.* **2015**, *27*, 676.

[5] N. Coppede, G. Tarabella, M. Villani, D. Calestani, S. Iannotta, A. Zappettini, *J. Mater. Chem. B* **2014**, *2*, 5620.

[6] P. Lin, X. Luo, I. M. Hsing, F. Yan, *Adv. Mater.* **2011**, *23*, 4035.

[7] C. Liao, M. Zhang, L. Niu, Z. Zheng, F. Yan, *J. Mater. Chem. B* **2014**, *2*, 191.

[8] D. Khodagholy, T. Doublet, P. Quilichini, M. Gurfinkel, P. Leleux, A. Ghestem, E. Ismailova, T. Hervé, S. Sanaur, C. Bernard, G. G. Malliaras, *Nat. Commun.* **2013**, *4*, 1575.

[9] P. Leleux, J. Rivnay, T. Lonjaret, J. M. Badier, C. Bénar, T. Hervé, P. Chauvel, G. G. Malliaras, *Adv. Healthcare. Mater.* **2015**, *4*, 142.

[10] D. Khodagholy, V. F. Curto, K. J. Fraser, M. Gurfinkel, R. Byrne, D. Diamond, G. G. Malliaras, F. B. Lopez, R. M. Owens, *J. Mater. Chem.* **2012**, *22*, 4440.

[11] A. Campana, T. Cramer, D. T. Simon, M. Berggren, F. Biscarini, *Adv. Mater.* **2014**, *26*, 3874.

[12] P. Andersson, D. Nilsson, P. O. Svensson, M. Chen, A. Malmström, T. Remonen, T. Kugler, M. Berggren, *Adv. Mater.* **2002**, *14*, 1460.

[13] C. B. Nielsen, A. Giovannitti, D. T. Sbircea, E. Bandiello, M. R. Niazi, D. A. Hanifi, M. Sessolo, A. Amassian, G. G. Malliaras, J. Rivnay, I. McCulloch, *J. Am. Chem. Soc.* **2016**, *138*, 10252.

[14] D. A. Bernards, G. G. Malliaras, *Adv. Funct. Mater.* **2007**, *17*, 3538.

[15] J. T. Friedlein, M. J. Donahue, S. E. Shaheen, G. G. Malliaras, R. R. Mcleod, *Adv. Mater.* **2016**, *28*, 8398.

[16] N. Coppedè, M. Villani, F. Gentile, *Sci. Rep.* **2014**, *4*, 4297.

[17] D. A. Bernards, D. J. Macaya, M. Nikolou, J. A. Defranco, S. Takamatsu, G. G. Malliaras, *J. Mater. Chem.* **2008**, *18*, 116.

[18] M. Kettner, I. Vladimirov, A. J. Strudwick, M. G. Schwab, R. T. Weitz, *J. Appl. Phys.* **2015**, *118*, 025501.

[19] P. Lin, F. Yan, J. Yu, H. L. W. Chan, M. Yang, *Adv. Mater.* **2010**, *22*, 3655.

[20] G. Tarabella, G. Nanda, M. Villani, N. Copped, R. Mosca, G. G. Malliaras, C. Santato, S. Iannotta, F. Cicoira, *Chem. Sci.* **2012**, *3*, 3432.

[21] V. Kaphle, S. Liu, A. Al-Shadeedi, C. M. Keum, B. Lussem, *Adv. Mater.* **2016**, *28*, 8766.

[22] K. J. Fraser, V. F. Curto, S. Coyle, B. Schazmann, R. Byrne, F. B. lopez, R. M. Owens, G. George, D. Diamond, *Proc. SPIE* **2011**, *8118*, 81180C-1.

[23] S. Y. Yang, F. Cicoira, R. Byrne, F. B. Lopez, D. Diamond, R. M. Owens, George G. Malliaras, *Chem. Commun*. **2010**, *46*, 7972.

[24] Q. Thiburce, L. Porcarelli, D. Mecerreyes, A. J. Campbell, *Appl. Phys. Lett.* **2017**, *110*, 233302.

[25] D. Wang, V. Noël, B. Piro, *Electronics* **2016**, 5, 9.

[26] M. Singh, K. Manoli, A. Tiwari, T. Ligonzo, C. D. Franco, N. Cioffi, G. Palazzo, G. Scamarcio, L. Torsi, *J. Mater. Chem. C* **2017**, *5*, 3509.

[27] J. H. Cho, J. Lee, Y. He, B. S. Kim, T. P. Lodge, C. D. Frisbie, *Adv. Mater.* **2008**, *20*, 686.

[28] S. Ono, S. Seki, R. Hirahara, Y. Tominari, J. Takeya, *Appl. Phys. Lett.* **2008**, *92*, 103313.

[29] Z. Yi, G. Natale, P. Kumar, E. D. Mauro, M. C. Heuzey, F. Soavi, I. I. Perepichka, S. K. Varshney, C. Santato, F. Cicoira, *J. Mater. Chem. C* **2015**, *3*, 6549.

[30] R. M. Owens, G. G. Malliaras, *MRS Bulletin* **2010**, *35,* 449.

[31] D. Khodagholy, J. Rivnay, M. Sessolo, M. Gurfinkel, P. Leleux, L. H. Jimison, E. Stavrinidou, T. Herve, S. Sanaur, R. M. Owens, G. G. Malliaras, *Nat. Commun.* **2013**, *4*, 2133.

[32] R. Memming, Semiconductor Electrochemistry; *Wiley VCH: Weinheim, Germany*, **2001**.

[33] E. Orgiu, S. Locci, B. Fraboni, E. Scavetta, P. Lugli, A. Bonfiglio, *Org. Electron.* **2011**, *12*, 477.

[34] Y. H. Noh, S. Young Park, S. M. Seo, H. H. Lee, *Org. Electron.* **2006**, *7*, 271.

[35] S. H. Kim, W. M. Yun, O. K. Kwon, K. Hong, C. Yang, W. S. Choi, C. E. Park, *J. Phys. D: Appl. Phys.* **2010**, *43*, 465102.

[36] F. Cicoira, M. Sessolo, O. Yaghmazadeh, J. A. Defranco, S. Y. Yang, G. G. Malliaras, *Adv. Mater.* **2010**, *22*, 1012.

[37] W. Xu, S. W. Rhee, *Org. Electron.* **2010**, *11*, 996.

[38] H. M. Yang, Y. K. Kwon, S. B. Lee, S. Kim, K. Hong, K. H. Lee, *ACS Appl. Mater. Interfaces* **2017**, *9*, 8813.

[39] K. K. Ryu, I. Nausieda, D. D. He, A. I. Akinwande, V. Bulović, C. G. Sodini, *IEEE Trans. Electron Devices* **2010**, *57*, 1003.

[40] H. Sinno, S. Fabiano, X. Crispin, M. Berggren, I. Engquist, *Appl. Phys. Lett.* **2013**, *102,* 113306.

[41] Q. Zhang, F. Leonardi, S. Casalini, I. Temiño, M. M. Torrent, *Sci. Rep.* **2016**, *6*, 39623.

[42] J. Lee, L. G. Kaake, J. H. Cho, X. Y. Zhu, T. P. Lodge, C. D. Frisbie, *J. Phys. Chem. C* **2009**, *113*, 8972.

[43] W. Xu, S.Y. Min, H. Hwang and T.W. Lee, *Sci. Adv.* **2016**, *2*, e1501326.

[44] Y. Burgt, E. Lubberman, E. J. Fuller, S. T. Keene, G.C.Faria, S. Agarwal, M. J. Marinella, A. A. Talin & A. Salleo, *Nat. Mater.* **2017**, *16*, 414.

[45] S. Zhang, E. Hubis, C. Girard, P. Kumar, J. DeFranco, F. Cicoira, *J. Mater. Chem.* **2016**, *4*, 1382.

[46] S. Zhang, E. Hubis, G. Tomasello, G. Soliveri, P. Kumar, F. Cicoira, Chem. Mater. **2017**, *29*, 3126.

[47] S. Liu, A. A. Shadeedi, V. Kaphle, C.M. Keum, B. Lussem, *Org. Electron*. **2017**, *45*, 124.